4.2 APPLICATION OF THE TOPKAPI MODEL WITHIN THE DMIP 2 PROJECT

Gabriele Coccia[(1)], Cinzia Mazzetti[(2)], Enrique A. Ortiz[(3)] and Ezio Todini[(1)]
[(1)]University of Bologna, Bologna, Italy
[(2)]ProGea Srl, Bologna, Italy
[(3)]HidroGaia, Paterna (Valencia), Spain

1 INTRODUCTION

The TOPKAPI (TOPographic Kinematic APproximation and Integration) model is a fully-distributed physically-based hydrologic model with a simple and parsimonious parameterization which simulates the rainfall runoff transformation using data collected by a network of rain-gauges.
The model is based on the idea of combining the Kinematic approach and the topography of the basin. Spatial distribution of catchment parameters, precipitation input and hydrologic response is achieved horizontally by an orthogonal grid network and vertically by soil layers at each grid pixel.
Three 'structurally similar' non-linear reservoir differential equations characterize the TOPKAPI approach and are used to describe subsurface flow, overland flow and channel flow. Moreover the TOPKAPI model includes components representing the primary processes of the hydrologic cycle: infiltration, percolation, evapo-transpiration and snowmelt, plus a lake/reservoir component, a parabolic routing component and a groundwater component.
Being a physically based model, the values of the model parameters can be easily derived from digital elevation maps, soil type and land use maps in terms of topology, slope, soil permeability, soil depth and superficial roughness. A calibration based on observed streamflow data is then necessary for 'fine tuning' the model to reproduce the behaviour of the catchment.
Thanks to its physically based parameters, the TOPKAPI model can be successfully implemented also in un-gauged catchments where the model cannot be calibrated using measured data. In this case the model parameters can be derived from thematic maps, literature and experience.
The present paper describes the structure of the TOPKAPI model and the results obtained in its application within the Distributed Model Intercomparison Project, Phase 2 (DMIP 2).

Corresponding authors address: Gabriele Coccia, Department of Earth and Geo-Environmental Sciences, Bologna University, 1 P.zza di P.ta S.Donato, 40126, Bologna, Italy; e-mail: gabriele.coccia4@unibo.it
Cinzia Mazzetti, ProGea Srl, 93 V. Galliera, 40121, Bologna, Italy; e-mail: cinzia.mazzetti@progea.net
Enrique A. Ortiz, HidroGaia, 27 S.L. Avenida Juan de la Cierva, 46980, Paterna (Valencia), Spain; e-mail: eortiz@hidrogaia.com
Ezio Todini, Department of Earth and Geo-Environmental Sciences, Bologna University, 1 P.zza di P.ta S.Donato, 40126, Bologna, Italy, e-mail: ezio.todini@unibo.it

2 THE TOPKAPI MODEL

2.1 The Soil Water Component

2.1.1 Basic Assumptions

The fundamental assumptions on which the TOPKAPI model is based, can be described as follows:

1) Precipitation is assumed to be constant over the integration domain (namely the single cell), by means of suitable averaging operations on the local rainfall data, such as Thiessen polygons techniques, Block Kriging (*de Marsily*, 1986; *Matheron*, 1970) or others;
2) <u>All the precipitation falling on the soil infiltrates into it, unless the soil is already saturated</u> in a particular zone (namely the single cell); this is equivalent to adopting the saturation mechanism from below as the sole mechanism for the formation of overland flow, ignoring on the other hand the possible activation of the Hortonian mechanism due to infiltration excess. This decision is justified by the fact that the infiltration excess mechanism is characteristic of a local modeling scale, whereas the saturation excess mechanism, being linked to a cumulative phenomenon and conditioned by a lateral redistribution movement of the water in the soil, becomes dominant as the scale of the modeling increases (*Blöschl and Sivapalan*, 1995).
3) The slope of the water table is assumed to coincide with the slope of the ground, unless the latter is very small (less than 0.01%); this constitutes the fundamental assumption of the approximation of the kinematic wave in the De Saint Venant equations, and it implies the adoption of a kinematic wave propagation model with regard to horizontal flow, or drainage, in the unsaturated area (*Henderson and Wooding*, 1964; *Beven*, 1981, 1982; *Borah et al.,* 1980; *Sloan and Moore*, 1984; *Hurley and Pantelis*, 1985; *Stagnitti et al.,* 1986; *Steenhuis et al.,* 1988);
4) Local transmissivity, like local horizontal flow, depends on the total water content of the soil, i.e. it depends on the integral of the water content profile in a vertical direction;
5) Saturated hydraulic conductivity is constant with depth in a surface soil layer but much larger than that of deeper layers; this forms the basis for the vertical aggregation of the transmissivity, and

therefore of the horizontal flow, as it will be described in details in the following section.

2.1.2 The Vertical Lumping

The transmissivity of a soil layer in non-saturated condition is given by the following expression:

$$T = \int_0^L k\left(\tilde{\vartheta}(z)\right)dz \tag{1}$$

Where: L = soil thickness of the layer affected by the horizontal flow.

$k\left(\tilde{\vartheta}(z)\right)$ = hydraulic conductivity in non-saturated conditions.

$\tilde{\vartheta} = \dfrac{\vartheta - \vartheta_r}{\vartheta_s - \vartheta_r}$ = reduced water content.

ϑ_r , ϑ_s = residual and saturated water content

ϑ = actual water content in the soil.

In accordance with the hypotheses 4) and 5) the transmissivity given by Eqn. ((1) can be replaced by the following approximated expression:

$$T\left(\tilde{\Theta}\right) = k_s L \tilde{\Theta}^{\alpha} \tag{2}$$

where k_s = saturated hydraulic conductivity.

$\tilde{\Theta} = \dfrac{1}{L}\int_0^L \tilde{\vartheta}(z)dz$ = mean value along the vertical profile of the reduced water content.

α = parameter depending on the characteristics of the soil (Benning, 1994; *Todini*, 1995).

The horizontal flux is calculated as follows, by means of an approximation of the Brooks and Corey's formula $k\left(\tilde{\vartheta}\right) = k_s \tilde{\vartheta}^{\alpha}$:

$$q = \tan(\beta) k_s L \tilde{\Theta}^{\alpha} \quad [\mathrm{m^2 s^{-1}}]. \tag{3}$$

where β = slope angle [rad].

α = parameter which depends on the soil characteristics.

2.1.3 Kinematic Wave Formulation for Sub-Surface Flow

The analysis of a generic hydraulic system is usually addressed using the continuity equation and the dynamic equation. In the TOPKAPI model, the dynamic equation is represented by an approximate form expressed by Eqn. (3). Combining Eqn. (3) with the equation for continuity of mass, the following system is obtained:

$$\begin{cases} (\vartheta_s - \vartheta_r) L \dfrac{\partial \tilde{\Theta}}{\partial t} + \dfrac{\partial q}{\partial x} = p \\ q = \tan(\beta) k_s L \tilde{\Theta}^{\alpha} \end{cases} \tag{4}$$

Where p is the intensity of precipitation [$\mathrm{ms^{-1}}$].

The model is written in just one direction since it is assumed that the flow along the slopes is characterized by a preferential direction, which can be described as the direction of maximum slope.

Eqn. (4) can be rewritten in terms of the actual total water content in the soil η:

$$\eta = (\vartheta_s - \vartheta_r) L \tilde{\Theta} \tag{5}$$

and making the following substitution:

$$C = \frac{L k_s \tan(\beta)}{(\vartheta_s - \vartheta_r)^{\alpha} L^{\alpha}} \tag{6}$$

The term C represents in physical terms a *local conductivity coefficient*, since it depends on soil parameters for a point position, which encompasses the effects of hydraulic conductivity and slope, to which it is directly proportionate, and storage capacity, to which it is inversely proportionate.

Eqn. (4), rewritten in terms of actual total water content in the soil, along the vertical profile, leads to the following Kinematic equation:

$$\frac{\partial \eta}{\partial t} = p - C \frac{\partial \eta^{\alpha}}{\partial x} \tag{7}$$

2.1.4 Non-Linear Reservoir Model for the Soil Water in a Generic Cell

By integrating Eqn. (7) in the soil over the *ith* DEM grid cell, whose space dimension is X, gives:

$$\frac{\partial v_{s_i}}{\partial t} = pX - \left(C_{s_i} \eta_i^{\alpha_s} - C_{s_{i-1}} \eta_{i-1}^{\alpha_s}\right) \tag{8}$$

where: v_s = volume of water per unit of width [$\mathrm{m^2}$].

X = grid cell dimension [m].

The subscript s is introduced here to distinguish this soil water equation from the ones relevant to the overland and the drainage network flows and will be kept from now on. The subscript i is introduced to highlight that the equation is referred to the *ith* cell and it will be omitted from now on.

In the TOPKAPI model, the grid cells are connected by a tree shaped network; water moves down slope along this tree shaped flow pathway starting from the initial cells (without upstream contributing areas) representing the ‘sources’ towards the outlet. According to this procedure, and assuming that in each cell the variation of the vertical water content along the cell is negligible, the volume of water stored in each cell (per unit width) can be related to the total water content, which is equivalent to the free water volume in depth, by means of the simple expression:

$$v_s = X\eta \tag{9}$$

Substituting for η in Eqn. (8) and writing it for a generic cell, given the total inflow to the cell, the following non-linear reservoir equation is obtained:

$$\frac{\partial V_s}{\partial t} = \left(pX^2 + Q_o^u + Q_s^u\right) - \frac{C_s X}{X^{2\alpha_s}} V_s^{\alpha_s} \tag{10}$$

where: V_s = volume of water stored in the *ith* DEM grid cell [$\mathrm{m^3}$].

pX^2 = precipitation on the *ith* DEM grid cell $[m^3s^{-1}]$.

Q_o^u = streamflow entering the active cell *i* as overland flow from the upstream contributing area $[m^3s^{-1}]$.

Q_s^u = streamflow entering the active cell *i* as sub-surface flow from the upstream contributing area $[m^3s^{-1}]$.

α_s = parameter which depends on the soil characteristics.

The volume of water stored in a cell can be related to the actual total water content by means of the following equation:

$$V_s = Xv_s = X^2\eta \tag{11}$$

Substituting Eqn. (11) into Eqn. (10) the differential equation for the soil component can be written as:

$$\frac{\partial\eta}{\partial t} = \frac{1}{X^2}\left(p\ X^2 + Q_o^u + Q_s^u\right) - \frac{C_s}{X}\eta^{\alpha_s} \tag{12}$$

In general Eqn. (12) can be written as:

$$\frac{\partial\eta}{\partial t} = a - b\eta^c \tag{13}$$

$$a = \frac{p\ X^2 + Q_o^u + Q_s^u}{X^2} = \frac{Q\_in}{X^2} \qquad b = \frac{C_s}{X} \qquad c = \alpha_s$$

Eqn. (13) can be solved analytically or numerically by means of the Runge-Kutta method.

2.1.5 Soil Water Balance

For the *ith* cell at each time step, the soil water balance can be calculated as follows:

$$Q_s^d = \left(pX^2 + Q_o^u + Q_s^u\right) - \frac{V_s\ (t_0 + dT) - V_s\ (t_0)}{dT} \tag{14}$$

where: Q_s^d = outflow from the *ith* cell during the time interval dT $[m^3s^{-1}]$.

pX^2 = water falling on the *ith* cell during the time interval dT $[m^3s^{-1}]$.

V_s = volume of water stored in the soil $[m^3]$.

In case of saturation of the soil cell the volume of water that exceeds the soil can be computed as follows:

$$Vexf_s = V_s\left(t_0 + dT\right) - Vsat_s$$

where: $Vexf_s$ = saturation excess volume for the *ith* cell $[m^3]$.

$Vsat_s$ = saturated soil water storage for the *ith* cell $[m^3]$.

2.1.6 Subsurface Flow in a Cell with General Inclination

If we consider a pixel with slope equal to $tg\beta_1$ in *x* direction and slope equal to $tg\beta_2$ in *y* direction the Eqn. (4) should be modified in the following way:

$$q = \tan\left(\beta_1\right)\left(1 + \frac{\tan\left(\beta_2\right)}{\tan\left(\beta_1\right)}\right)k_s L\tilde{\Theta}^{\alpha} \tag{15}$$

As a consequence also the local conductivity coefficient C_s will be modified:

$$C_s = \tan(\beta_1)\left(1 + \frac{\tan(\beta_2)}{\tan(\beta_1)}\right)\frac{Lk_s}{\left(\vartheta_s - \vartheta_r\right)^{\alpha}L^{\alpha}} \tag{16}$$

With: $$\sigma_s = 1 + \frac{\tan(\beta_2)}{\tan(\beta_1)} \tag{17}$$

The coefficient σ_S will be called *soil drainage coefficient*. Eqn. (13) representing the non-linear reservoir for the subsurface flow component will be modified in the following way:

$$\frac{\partial\eta}{\partial t} = a - \sigma_s b\eta^c \tag{18}$$

From Eqn. (18) the total outflow Q_{out} from the soil is computed. Then the outflow is partitioned between the downstream cell and the channel network, according to the flow partition coefficient.

2.2 The Surface Water Component

The input to the surface water model is the *precipitation excess* resulting from the saturation of the surface soil layer. In addition, water in the soil can exfiltrate on the surface as return flow due to a sudden change in hill slope or soil properties, and thus it can also feed the overland flow. The subsurface flow and the overland flow together feed the channel along the drainage network.

Overland flow routing is described similarly to the soil component, according to the kinematic approach (*Wooding*, 1965), in which the momentum equation is approximated by means of the Manning's formula. For a general cell, the kinematic wave approximation for overland flow is described as:

$$\begin{cases} \dfrac{\partial h_o}{\partial t} = r_o - \dfrac{\partial q_o}{\partial x} \\ q_o = \dfrac{1}{n_o}(\tan\beta)^{\frac{1}{2}} h_o^{\frac{5}{3}} = C_o h_o^{\alpha_o} \end{cases} \tag{19}$$

where: h_o = water depth over the ground surface [m].

r_o = saturation excess resulting from the solution of the soil water balance either as precipitation or exfiltration from the soil in absence of rainfall $[ms^{-1}]$.

q_o = horizontal flow on the ground surface, corresponding to a streamflow per unit of width $[m^2s^{-1}]$.

n_o = Manning's friction coefficient for the surface roughness $[m^{-1/3}s]$.

α_o = exponent that derives from using Manning's formula, equal to 5/3.

$C_o = \frac{\tan(\beta)^{1/2}}{n_0}$ = coefficient relevant to Manning's formula for overland flow.

A subscript *o* denotes the overland flow. Eqn. (19), leads to the following kinematic equation:

$$\frac{\partial h_o}{\partial t} = r_o - C_o \frac{\partial\left(h_o^{\alpha_O}\right)}{\partial x} \tag{20}$$

By analogy with what was done for the soil, assuming the surface water depth constant over the cell and integrating the kinematic equation over the longitudinal dimension, the non-linear reservoir equation for the overland flow for the *ith* cell can be obtained as:

$$\frac{\partial V_{o_i}}{\partial t} = r_{o_i} X W_{o_i} - \frac{C_{o\,i} W_{o_i}}{\left(X W_{o_i}\right)^{\alpha_o}} V_{o_i}^{\alpha_o} \tag{21}$$

where V_o = surface water volume in the cell [m^3].
W_o = width of the surface (free of the channel) [m].

The subscript *i* is introduced here to highlight that Eqn. (21) was written for the *ith* DEM grid cell and it will be omitted from now on. The volume of water stored on the surface of each cell can be written through a simple expression:

$$V_o = X W_o h_o \tag{22}$$

Substituting Eqn. (22) into Eqn. (21) the differential equation for the surface component can be written as:

$$\frac{\partial h_o}{\partial t} = r_o - \frac{C_o}{X} h_o^{\alpha_O} \tag{23}$$

In general Eqn. (23) can be written as:

$$\frac{\partial h_o}{\partial t} = a - b h_o^c \tag{24}$$

$$a = r_o = \frac{1}{X W_o} \frac{Vexf}{dT} \qquad b = \frac{C_o}{X} = \frac{\tan(\beta)^{1/2}}{n_o X} \qquad c = \alpha_o$$

where: V_{exf} = precipitation excess [m^3]

Eqn. (23) can be solved numerically (Runge-Kutta) or analytically.

2.2.1 Surface Water Balance

For the *ith* cell at each time step, the surface water balance can be calculated as follows:

$$Q_o^d = \left(r_o\, X W_o\right) - \frac{V_o\,(t_0 + dT) - V_o(t_0)}{dT} \tag{25}$$

where: Q_o^d = outflow from the *ith* cell during the time interval T [m^{3}s^{-1}].
$r_o X W_o$ = inflow into the *ith* cell during the time interval dT [ms^{-1}].
V_o = volume of water on the surface [m^3].

Up to this point it has been implicitly assumed that the entire overland flow from a cell flows into the downstream cell immediately. However, this is not entirely true since note has to be taken of the depletion caused by the drainage network. Thus, for the cells in the channel network, the overland flow is still evaluated by Eqn. (23), but it is then partitioned between the channel and the downstream cell. This allows determination of the amount of overland flow feeding the drainage channel network.

2.2.2 Overland Flow in a Cell with General Inclination

If we consider a pixel with slope equal to $tg\beta_1$ in *x* direction and slope equal to $tg\beta_2$ in *y* direction the Eqn. (19) should be modified in the following way:

$$q_o = \frac{1}{n_o} (\tan\beta_1)^{\frac{1}{2}} \left[1 + \left(\frac{\tan\beta_2}{\tan\beta_1} \right)^{\frac{1}{2}} \right] h_o^{\frac{5}{3}} \tag{26}$$

$$\sigma_o = 1 + \left(\frac{\tan(\beta_2)}{\tan(\beta_1)} \right)^{\frac{1}{2}} \tag{27}$$

The coefficient σ_O will be called *surface drainage coefficient*. Eqn. (13) representing the non-linear reservoir for the overland flow component will be modified in the following way:

$$\frac{\partial h_o}{\partial t} = a - \sigma_o b h_o^c \tag{28}$$

From Eqn. (28) the total outflow Q_{out} from the overland flow is computed. Then the outflow is partitioned between the downstream cell and the channel network according to the flow partition coefficient.

2.3 The Channel Component

In the TOPKAPI model, different kinds of channel cross section geometries can be set; following, a rectangular cross section will be used as an example to describe the channel component structure.

2.3.1 Channels with Rectangular Cross Sections

The channel flow is described similarly to the surface component, although in this case the channel is assumed to be tree shaped with reaches having rectangular cross sections.

The kinematic wave approximation for the channel flow is described according to the kinematic approach in which the momentum equation is approximated by means of the Manning's formula:

$$\begin{cases} \dfrac{\partial V_c}{\partial t} = \left(r_c + Q_c^u\right) - q_c \\ q_c = \dfrac{1}{n_c}\sqrt{s_0}\left(\dfrac{A_x}{C_x}\right)^{2/3} B_x y_c^{\frac{5}{3}} \end{cases} \tag{29}$$

where: y_c = water depth in the channel reach [m].
r_c = lateral drainage input, including the surface runoff and the soil drainage reaching the channel [m^{3}s^{-1}].
$Q^u{}_c$ = inflow from the channel reach of the upper cell [m^{3}s^{-1}].

q_c = horizontal flow in the channel [m^{3}s^{-1}].
n_c = Manning's friction coefficient [$m^{-1/3}s$].
s_0 = bed slope.
A_x = wet area [m^2], C_x = wet contour [m]
B_x = width of the channel reach [m].

A subscript *c* denotes the channel flow. Eqn. (29) , rewritten in terms of water depth in the channel reach, y_c, leads to the following equation:

$$\frac{\partial V_c}{\partial t} = \left(r_c + Q_c^u\right) - \frac{\sqrt{s_0}}{n}\left(\frac{B_x}{C_x}\right)^{2/3} B_x y_c^{\frac{5}{3}} \tag{30}$$

With simple substitutions we obtain the following equation that describes the non-linear reservoir equation for the channel flow for the *ith* cell:

$$\frac{\partial V_c}{\partial t} = \left(r_c + Q_c^u\right) - \frac{\sqrt{s_0}}{n}\left(\frac{B_x}{C_x}\right)^{2/3} \frac{1}{B^{\frac{2}{3}} X^{\frac{5}{3}}} V_c^{\frac{5}{3}} \tag{31}$$

In general Eqn. (31) can be written as:

$$\frac{\partial V_c}{\partial t} = a - bV_c^c \tag{32}$$

$$a = r_c + Q_c^u \qquad b = \frac{\sqrt{s_0}}{n_c}\left(\frac{1}{C_x'}\right)^{2/3} \frac{1}{X^{5/3}} \qquad c = \frac{5}{3}$$

where: $A_x' = B \cdot y_{c_0}$ = wet area at the beginning of the computation time step [m^2].
$C_x' = 2y_{c_0} + B$ = wet contour at the beginning of the computation time step [m].

The channel width *B* is increasing as a function of the area drained by the *ith* cell on the basis of geo-morphological considerations.

2.3.2 Channel Water Balance

For the *ith* cell at each time step, the channel water balance can be calculated as follows:

$$Q_c^d = \left(r_c XW + Q_c^u\right) - \frac{V_c\left(t_0 + dT\right) - V_c\left(t_0\right)}{dT} \tag{33}$$

where: Q_c^d = outflow [m^{3}s^{-1}].
$r_c XW_o$ = inflow from the lateral cells [m^{3}s^{-1}].
Q_c^u = inflow from the upper cell [m^{3}s^{-1}].
V_o = volume of water in the channel [m^3].

2.4 Analytical Solution of the Non-Linear Reservoir Ordinary Differential Equation (ODE)

As described in the previous paragraphs, the TOPKAPI model formulation leads to three tree-shaped cascades of non-linear reservoirs, each of which is described by a "structurally similar" ordinary differential equation (ODE) to be solved in time. In the first version of the TOPKAPI model (*Todini and Ciarapica*, 2001), the solution of the ODE for each single reservoir representing the soil, the surface and the channel network, was based upon a variable step fifth order Runge-Kutta numerical algorithm due to *Cash and Karp* (1990). Nowadays, it has been found that the non-linear reservoir equation can be solved analytically based on an appropriate approximation (*Liu and Todini,* 2001).

2.5 The Muskingum-Cunge-Todini Routing Method

In the TOPKAPI model it is possible to use the Muskingum-Cunge-Todini (MCT) (*Todini*, 2007) routing method as an alternative to the Kinematic non-linear reservoir for channels with slope smaller than 0.1%, namely channels where the Kinematic approximation of De Saint-Venant equations does not hold.

The Muskingum-Cunge (MC) routing method (*Cunge*, 1969; *Ponce and Yevjevich*, 1978; *Koussis*, 1980, 1983; *Miller and Cunge*, 1975; *Wienmann and Laurenson*, 1979) is actually a lumped Kinematic wave routing method, in which the Kinematic wave equation is transformed into an equivalent diffusive wave equation by matching the physical diffusion to the numerical diffusion resulting from the imperfectly centered finite difference scheme (*Smith*, 1980; *Tang and Samuels*, 1999). Thus the MC method accounts for both the convection and diffusion of the flood wave. The routing parameters can be linked to physical channel properties and flow characteristics (*Cunge*, 1969), and when these parameters are recalculated and updated as a function of local flow values for each computational cell, the routing parameters are varying in time (*Prince*,1995). The MCT algorithm, is basically a variable parameter MC corrected for its typical mass balance error (*Todini*, 2007).

2.6 The Evapo-Transpiration Component

The evapo-transpiration is taken into account as water loss, subtracted from the soil's water balance. A simplified technique is used to calculate evapo-transpiration starting from air temperature and from other topographic, geographic and climatic information. The effects of the vapour pressure and wind speed are explicitly ignored. In the TOPKAPI model, the evapo-transpiration is evaluated at the DEM grid scale.

2.6.1 Empirical Equation for Computing the Reference Potential Evapo-Transpiration

An empirical equation, that relates the reference potential evapo-transpiration ET_{0m}, to the compensation factor *Wta*, to the mean recorded temperature of the month T and the maximum number of hours of sunshine N of the month, was developed. The reference potential evapo-transpiration is computed on a monthly basis using one of the available simplified expressions such as for instance the one due to *Thornthwaite and Mather* (1955). The developed relationship is linear in temperature (and hence additive) and allows the unbundling of the monthly results on daily or hourly basis, while most

other empirical equations are ill-suited for time intervals shorter than one month.
The relation used, which is structurally similar to the radiation method formula (*Doorembos et al.*, 1984) in which the air temperature is taken as an index of radiation, is:

$$ET_{0m} = \alpha + \beta N W_{ta} T_m \tag{34}$$

Where: ET_{0m} = reference evapo-transpiration for a monthly time step (computed using Thornthwaite's formula) [mm]
α, β = regression coefficients to be estimated
T_m = area mean air temperature averaged over a month [°C]
N = monthly mean of the maximum number of daily hours of sunshine (tabulated as a function of latitude)
W_{ta} = weighting factor, it can be either obtained from tables or approximated by a fitted parabola:

$$W_{ta} = A\overline{T}^2 + B\overline{T} + C$$

A, B, C = coefficients to be estimated
$\overline{T}$ = mean monthly temperature [°C]

For a given time step Δt and a given crop culture, the potential evapo-transpiration value is computed as:

$$ET_0 = K_c(\alpha + \beta N W_{ta} T_{\Delta t})\frac{\Delta t}{30 \cdot 24 \cdot 3600} \tag{35}$$

where: ET_0 = reference evapo-transpiration for a specified time step Δt [mm].
K_c = crop factor.
α, β = regression coefficients.
$T_{\Delta t}$ = pixel mean air temperature averaged over Δt [°C].

2.6.2 Estimation of the Average Monthly Potential Evapo-Transpiration According to Thornthwaite

The values of the potential evapo-transpiration can be computed for a given DEM grid according to Thornthwaite, by means of the following formula:

$$ET_{0m}(i) = 16a(i)\left[10\frac{T(i)}{b}\right]^c \tag{36}$$

$$a(i) = \frac{n(i)}{30}\frac{N(i)}{12} \quad b = \sum_{i=1}^{12}\left[\frac{T(i)}{5}\right]^{1.514}$$

$$c = 0.49239 + 1792 \times 10^{-5} b - 771 \times 10^{-7} b^2 + 675 \times 10^{-9} b^3$$

where: $ET_{m0}(i)$ = average monthly potential evapo-transpiration [mm/month].
$T(i)$ = monthly-average air temperature for *ith* month [° C].
$n(i)$ = number of days in month *i.*
$N(i)$ = Mean Daily Duration of Maximum Possible Sunshine Hours (in 'Crop Water Requirements' FAO Irrigation and Drainage Paper 24).

2.6.3 Computation of the Actual Evapo-Transpiration

The potential evapo-transpiration is corrected as a function of the actual soil moisture content, to obtain the actual evapo-transpiration (ETa):

$$ETa = 0 \qquad \text{for } V \le \beta_1 V_{sat}$$

$$ETa = ET_0 \frac{V}{V_{sat}} \qquad \text{for } \beta_1 V_{sat} \le V \le \beta_2 V_{sat}$$

$$ETa = ET_0 \qquad otherwise$$

where: V, V_{sat} = actual and saturation volume of water into the soil [m^3].
β_1, β_2 = parameters to be fixed.

2.7 The Snow Accumulation and Snow Melting Component

The snowmelt module of the TOPKAPI model is driven by a radiation estimate based upon the air temperature measurements; in practice, the inputs to the module are the precipitation, the temperature, and the same radiation approximation which was used in the evapo-transpiration module.
The snowmelt module consists of the following steps.

2.7.1 Estimation of Solar Radiation

The estimation of the solar radiation at the DEM is performed by re-converting the latent heat and the sensible heat, assumed equals to the reference evapo-transpiration back into radiation, by means of a conversion factor C_{er} (Kcal Kg^{-1}):

$$C_{er} = 606.5 - 0.695(T - T_0) \tag{37}$$

where: C_{er} = conversion factor [Kcal Kg^{-1}].
T_0 = fusion temperature of ice [273 °K].
T = air temperature [° K].

In addition, to account for albedo, which plays an extremely important role in snowmelt, it is necessary to apply an efficiency factor which will be assumed approximately as η=0.6 for clear sky and η=0.8 for overcast conditions. Moreover, a coefficient η_{rad} is used to take in account the radiation efficiency; it depends on the sun height with respect to the terrain slope. This leads to the following estimate for the driving radiation term:

$$Rad = 2\eta_{al}\eta_{rad}\left[606.5 - 0.695(T - T_0)\right]ET_0 \tag{38}$$

where: Rad = radiation term.
η_{al} = efficiency factor for albedo.
η_{rad} = radiation efficiency factor.
ET_0 = potential evapo-transpiration.

2.7.2 Computation of the Solid and Liquid Percentage of Precipitation

The percentage of liquid precipitation is calculated by means of a function of the air temperature:

$$F(T) = \frac{1}{1 + e^{-\frac{T - T_s}{\sigma}}} \tag{39}$$

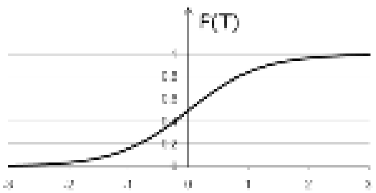

Figure 1 - Percentage of liquid precipitation for T_S=0

where σ is equal to 0.3 (derived by experimental data) and the value of T_S (which generally ranges between 271 and 275 °K) must be derived, as previously mentioned, by plotting the frequency of the status of historically recorded precipitation as a function of air temperature.

2.7.3 Estimation of the Water and Energy Budgets on the Hypothesis of Zero Snowmelt

The water equivalent mass (*Z*) is estimated with the following simple mass balance equation:

$$Z^*_{t+\Delta t} = Z_t + P \tag{40}$$

where *P* is the precipitation.
The water equivalent at the end of the time step is identified with a star, because it is a tentative value which does not yet account for the eventual snowmelt.
Similarly to the mass, the energy is estimated in the following way, by computing the increase (or decrease) of total energy (*E*):

$$\begin{aligned} E^*_{t+\Delta t} &= E_t + Rad + C_{si} T \cdot [1 - F(T)] \cdot P + \\ &+ [C_{si} T_0 + C_{lf} + C_{sa}(T - T_0)] \cdot P \cdot F(T) \end{aligned} \tag{41}$$

where: C_{si}= specific heat of ice
C_{lf} = latent heat of fusion of water
C_{sa} = specific heat of water

2.7.4 Estimation of Snowmelt and Updating of Mass and Energy Budgets

If the total available energy is smaller or equal to that required to maintain the total mass in the solid phase at the temperature T_0 i.e: $C_{si} Z^*_{t+\Delta t} T_0 \geq E^*_{t+\Delta t}$, it means that the available energy is not sufficient to melt part of the accumulated snow, and therefore:

$$\begin{cases} R_{sm} = 0 \\ Z_{t+\Delta t} = Z^*_{t+\Delta t} \\ E_{t+\Delta t} = E^*_{t+\Delta t} \end{cases} \tag{42}$$

where: R_{sm} = snowmelt [mm]
If the total available energy is larger than that required to maintain the total mass in the solid phase at the temperature T_0, it means that part of the accumulated snow will melt, and therefore the following energy balance equation holds:

$$C_{si}\left(Z^*_{t+\Delta t} - R_{sm}\right) T_0 = E^*_{t+\Delta t} - \left(C_{si} T_0 + C_{lf}\right) R_{sm} \tag{43}$$

from which the snowmelt and the mass and energy state variables can be computed as:

$$\begin{cases} R_{sm} = \dfrac{E^*_{t+\Delta t} - C_{si} T_0 Z^*_{t+\Delta t}}{C_{lf}} \\ Z_{t+\Delta t} = Z^*_{t+\Delta t} - R_{sm} \\ E_{t+\Delta t} = E^*_{t+\Delta t} - \left(C_{si} T_0 + C_{lf}\right) R_{sm} \end{cases} \tag{44}$$

2.8 The Percolation Component

For the deep aquifer flow, the response time related to the vertical transport of water through the thick soil above this aquifer is so large that horizontal flow in the aquifer can be assumed to be almost constant with no significant response on one specific storm event in a catchment (*Todini*, 1995). Nevertheless, the TOPKAPI model accounts for water percolation towards the deeper subsoil layers even though it does not contribute to the streamflow.
It is assumed that percolation starts if the soil moisture content of the upper soil layer exceeds its field capacity. The percolation rate from the upper soil layer is assumed to increase as a function of the soil water content, according to an experimentally determined power law (*Clapp and Hornberger*, 1978; *Liu et al.*, 2005).

$$P_r = k_{sv} \left(\frac{v}{v_{sat}} \right)^{\alpha_p} \tag{45}$$

where: P_r = percolation [mm]
k_{sv} = vertical soil saturated hydraulic conductivity
v = volume of water [m^3]
v_{sat} = local saturation volume [m^3]
α_p = exponent depending on the type of the soil ($\alpha_p \approx 11$ for sand; $\alpha_p \approx 25$ for clay)

3 APPLICATION OF THE TOPKAPI MODEL WITHIN THE DMIP 2 PROJECT

Within the DMIP 2 Project, the TOPKAPI model has been applied to the Sierra Nevada basins: the American River and the Carson River. These basins are geographically close, but their hydrological regimes are quite different; the Carson River basin is a high altitude basin with a snow dominated regime, while the American River drains an area that is lower in elevation with precipitation falling as rain and mixed snow and rain (*Jeton et al.*, 1996), Details on the basins features are available in (*Smith et al.*, 2006).

3.1 Data Description

TOPKAPI model input is made of a few data: the Digital Elevation Model, the soil type grid, the land use grid and the hydro-meteorological data, such as rain and temperature grids, or rain gauge and thermometer measurements, and observed streamflow.

3.1.1 Digital Elevation Model

The resolution of the used DEM was set to 250 m resolution, with UTM coordinates reference system (Figures 2 and 4); this resolution has been adopted for all the terrain maps. The DEM has been treated by some pre-processors that allows to eliminate the *false outlets* and the *sinks.* The formers are the cells on the basin boundary with elevation lower than the surrounding cells and different from the real outlet cell, which corresponds to the basin closure; these cells would generate inexistent points of outflow. The latters are the cells inside the basin with elevation lower than the surrounding cells. This situation is not allowed because each cell needs one outflow direction defined by the elevation. In both cases the elevation cell is set equal to the elevation of the lowest neighbouring cell. So the flow direction and the basin closure cell are uniquely indentified.
Moreover, the DEM was 'excavated' next to the river bed to help the pre-processor indentifying the stream network, which is automatically estimated with excellent precision.

3.1.2 Soil Type

The soil type classes were defined by the data developed by Miller and White (1998) and available on line at the Penn State Center for Environmental Informatics Database, dbwww.essc.psu.edu. The grids contain the dominant soil texture class for each

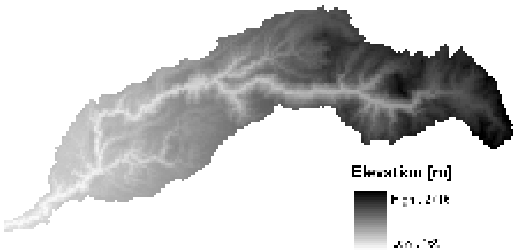

Figure 2 – DEM grid of the American River

of the 11 standard soil layers derived from State Soil Geographic (STASGO) soil data, compiled by the Natural Resources Conservation Service (NRCS) of the U.S. Department of Agriculture. Soil parameters value has been assigned for every SATSGO soil texture class, using the USDA soil texture class index by referring to the USDA parameters table for the Green-Ampt (*Maidment*, 1993) infiltration model (Table 3).
For both the basins, areas with the same layers alternation have been identified looking at the grids of the 11 soil layers. Hence, another soil classification based on those new soil classes (Tables 1 and 2) has been defined. The corresponding soil type grids are shown in Figure 3 and Figure 5.

Figure 3 – Soil Type grid of the American River

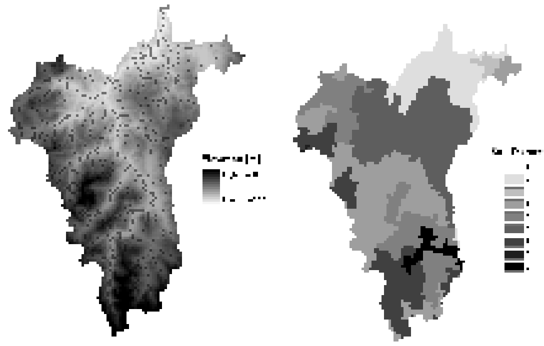

Figure 4, 5 – DEM grid (left) and Soil type grid (right) of the Carson River

Table 1 – Soil Type Classes used on the Carson River, alternation of the SATSGO soil texture classes

	Class	1	2	3	4	5	6	7	8	9
Depth Layers [cm]	0-5	6a	3a	3a	3a	1a	3a	16a	3a	3a
	05-10	12a	3a	2a	3a	1a	3a	16a	3a	3a
	10-20	12a	12a	3a	3a	1a	3a	16a	3a	3a
	20-30	12a	12a	3a	3a	1a	6a	16a	3a	3a
	30-40	12a	12a	3a	3a	16a	6a	16a	3a	3a
	40-60	16a	16a	3a	3a	16a	6a	16a	3a	3a
	60-80	15a	15a	3a	3a	15a	6a	16a	3a	3a
	80-100	15a	15a	3a	3a	15a	16a	16a	3a	15a
	100-150	15a	15a	3a	15a	15a	15a	16a	16a	15a

Table 2 – Soil Type Classes used on the American River, alternation of the SATSGO soil texture classes

	Class	1	2	3	4	5	6	7	8	9	10	11
Depth Layers [cm]	0-5	3a	6a	3a	6a	3a	3a	6a	16a	3a	6a	4a
	5-10	3a	6a	3a	6a	3a	3a	6a	16a	3a	4a	6a
	10-20	3a	4a	6a	6a	3a	3a	6a	16a	3a	4a	6a
	20-30	3a	4a	6a	6a	3a	3a	6a	16a	3a	4a	6a
	30-40	3a	16a	6a	6a	3a	3a	6a	16a	3a	16a	6a
	40-60	3a	16a	4a	9a	3a	3a	9a	16a	3a	16a	9a
	60-80	3a	16a	16a	9a	3a	3a	9a	16a	16a	15a	9a
	80-100	3a	15a	15a	9a	3a	15a	15a	16a	15a	15a	15a
	100-150	16a	15a	15a	9a	15a	15a	15a	16a	15a	15a	15a

Table 3 – Parameters value assigned to the STASGO soil texture classes

Soil Texture Class	Description	K_{sh} [ms^{-1}]	ϑ_s	ϑ_r	n	α	K_{sv} [ms^{-1}]
1a	Sand	5.42756E-05	0.3791	0.0497	2.8797	11.1000	5.42756E-08
2a	Loamy sand	1.30568E-05	0.3832	0.0431	1.7778	11.7600	1.30568E-08
3a	Sandy loam	3.99694E-06	0.3885	0.0413	1.4139	12.8000	3.99694E-09
4a	Silt loam	2.92556E-06	0.4440	0.0603	1.6949	13.7800	2.92556E-09
5a	Silt	5.60222E-06	0.5038	0.0486	1.6748	13.6000	5.60222E-09
6a	Loam	1.23781E-06	0.4005	0.0586	1.4869	18.0000	1.23781E-09
7a	Sandy clay loam	1.40475E-06	0.4766	0.0909	1.4923	20.0400	1.40475E-09
8a	Silty clay loam	1.40547E-06	0.3886	0.0689	1.3050	17.2400	1.40547E-09
9a	Clay loam	7.91543E-07	0.4385	0.0825	1.3884	18.5000	7.91543E-10
10a	Sandy clay	1.97124E-06	0.4030	0.0825	1.2063	23.8000	1.97124E-09
11a	Silty clay	1.78997E-06	0.5051	0.1024	1.3598	23.8000	1.78997E-09
12a	Clay	2.02196E-06	0.4801	0.0962	1.2100	25.8000	2.02196E-09
15a	Bedrock						
16a	Other	7.53998E-06	0.4326	0.0688	1.5741	17.5183	7.53998E-09

Table 4 – Parameters value of the land use, or vegetation, classes used in both the basins

			CROP FACTORS											
NAME	**ID**	**MANNING COEFFICIENT**	**JAN**	**FEB**	**MAR**	**APR**	**MAY**	**JUN**	**JUL**	**AUG**	**SEP**	**OCT**	**NOV**	**DEC**
WATER	**0**	0.03	1.05	1.05	1.05	1.05	1.05	1.05	1.05	1.05	1.05	1.05	1.05	1.05
EVERGREEN NEEDLELEAF FOREST	**1**	0.22	0.90	0.90	0.90	0.90	0.90	0.90	0.90	0.90	0.90	0.90	0.90	0.90
DECIDUOUS BROADLEAF FOREST	**4**	0.28	0.60	0.70	0.95	1.05	1.05	0.80	0.80	0.80	0.80	1.20	1.10	0.60
MIXED FOREST	**5**	0.28	0.75	1.00	0.90	0.95	1.20	0.85	0.85	0.85	0.85	1.05	1.00	0.75
WOODLAND	**6**	0.16	0.75	1.00	0.90	0.95	1.20	0.85	0.85	0.85	0.85	1.05	1.00	0.75
WOODED GRASSLAND	**7**	0.10	0.80	1.05	1.10	1.10	1.10	0.80	0.90	0.80	0.80	1.00	1.00	0.90
CLOSED SHRUBLAND	**8**	0.10	0.60	0.65	0.70	0.75	0.80	0.80	0.85	0.85	0.85	0.80	0.80	0.60
OPEN SHRUBLAND	**9**	0.10	0.60	0.65	0.70	0.75	0.80	0.80	0.85	0.85	0.85	0.80	0.80	0.60
GRASSLAND	**10**	0.10	0.80	1.05	1.10	1.10	1.10	0.80	0.90	0.80	0.80	1.00	1.00	0.90
CROPLAND	**11**	0.10	0.70	1.00	1.10	1.20	1.35	1.20	1.10	0.90	1.30	1.25	1.20	0.75

3.1.3 Land Use

The land use grids provided by the DMIP 2 have been used without modifications (Figures 6 and 7). The TOPKAPI model needs, for each land use class, the roughness parameter (Manning coefficient) and the crop factor values for every month. In Table 4 the parameters assigned for each land use class are shown.

Figure 6 – Land Use grid of the American River

3.1.4 Hydro-Meteorological Data

Available meteorological data were hourly rain and temperature grids between 01/01/1987 and 31/12/2002, produced from the NOAA'a National Weather Service, with a 4 km resolution. For the Carson river, the hydrological data were the observed streamflow in two measurement stations, namely Markleeville, CA and Gardnerville, NV, between

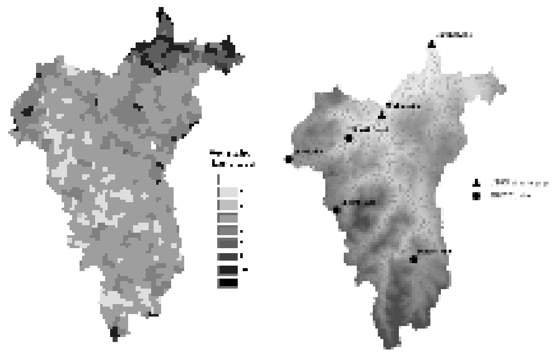

Figure 7, 8 – Land Use grid (left) and Stream gage and SNOTEL site (right) of the Carson River

01/10/1990 and 30/09/1997 and the snow water equivalent data measured in four stations, namely Blue Lake, Ebbetts Pass, Poison Flats and Spratt Creek, during the same period (Figure 8). For the American river, the hydrological data were the observed streamflow at the measurement station of

North Fork Dam, CA between 01/10/1988 and 30/09/1997 and the snow water equivalent data measured in two stations, namely Blue Canyon and Huysink, during the same period (Figure 9).
Summarizing, the available data allow to calibrate the model during a long period of about 10 years. The remaining 5 years of meteorological data will be used for the model validation. The validation period data have been submitted to the DMIP 2, but the results are not available, yet. The next paragraphs will only discuss the calibration results.

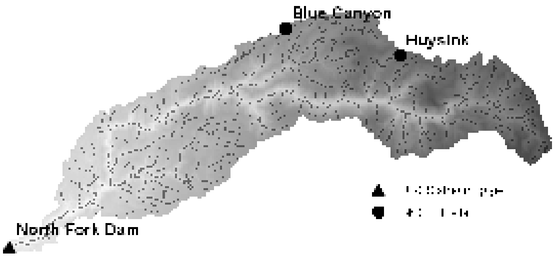

Figure 9 – Stream gage and SNOTEL site on the American River

3.2 Model Calibration

The model calibration was performed at a 1-hour time-step using the hydrometerological dataset previously described.
The initial soil saturation percentage was set to the same value of 0.9 for all cells at the beginning of the calibration period. It was assumed that no snow or surface water was over the slopes and the water depth in a generic channel cell increased linearly with the channel width. The observed streamflow data were available since October 1, 1990 for the Carson River and since October 1, 1989 for the American River; the meteorological dataset until these dates was used as model 'warm-up' period, so it is reasonable to assume that at the beginning of the calibration period, the simulated catchment state was representative of the real state.
The initial values of the soil parameters for each soil class are illustrated in Tables 5 and 6.
The soil calibrated parameter values are shown in Tables 7 and 8 and they were obtained by a 'trial and error' method based on the comparison between the simulated and the observed streamflows.
The roughness of channel flow was estimated by referring to Chow (1959), Barnes (1967) and Maidment (1993), according to the Strahler channel order (Strahler, 1957) (Table 9).
The evapo-transpiration and snowmelt modules parameters are shown in Table 10.
Using the calibrated model parameter values, the TOPKAPI could be validated using the dataset related to the period between October 1, 1997 and December 31, 2002.
As shown in Tables 5, 6, 7 and 8, the parameters which have been most modified during the calibration were the horizontal and vertical saturated conductivity and the thickness of the soil, while the land use parameters, the surface and channel roughness have not be changed with respect to the initial values.
The snow formation threshold was imposed greater than 0 and similar values of the evapotranspiration parameters were used in both basins.

3.3 Calibration Results

In this paragraph, the calibration results obtained for the streamflow measurement station available on the American River (North Fork Dam) and the two available on the Carson River (Gardnerville and Markleeville) will be discussed. The results are illustrated by figures depicting the comparison between the observed streamflow series, the simulated streamflow series with calibrated parameters and the simulated streamflow series with uncalibrated parameters.
Each figure corresponds to a main event or a significant long term simulation period (Tables 10 and 16). For all the selected events, the following evaluation indexes are calculated: Percent Bias (*PB*), Correlation Coefficient (*r*), Modified Correlation Coefficient (r_{mod}), Nash-Sutcliffe Efficiency (*NS*) (*Smith et al.*, 2004) and Explained Variance (*EV*). The same indexes are shown for the overall data and for individual year.
Moreover, an events analysis is computed considering the main events for the whole calibration period (Tables 12 and 18) and computing the following event evaluation indexes: Percent Absolute Event Runoff Error (*ER*), Percent Absolute Peak Error (*EP*), Percent Absolute Peak Time Error (*ET*) (*Smith et al.*, 2004).

Table 5 – Uncalibrated soil parameters value, Carson River

Class	Depth [m]	ϑ_s	ϑ_r	K_{sh} [ms^{-1}]	n	α	K_{sv} [ms^{-1}]
1	0.6	0.4576	0.0839	3.80E-06	1.3545	22.39	3.80E-09
2	0.6	0.4490	0.0779	4.19E-06	1.3654	20.87	4.19E-09
3	1.5	0.3883	0.0414	4.30E-06	1.4260	12.77	4.30E-09
4	1.0	0.2331	0.0413	4.00E-06	1.4139	12.80	4.00E-09
5	0.6	0.4058	0.0592	3.09E-05	2.2269	14.31	3.09E-08
6	1.0	0.4045	0.0572	3.05E-06	1.4897	16.86	3.05E-09
7	1.5	0.4326	0.0688	7.54E-06	1.5741	17.52	7.54E-09
8	1.5	0.4032	0.0505	5.18E-06	1.4673	14.37	5.18E-09
9	0.8	0.3885	0.0413	4.00E-06	1.4139	12.80	4.00E-09

Table 6 – Uncalibrated soil parameters value, American River

Class	Depth [m]	ϑ_s	ϑ_r	K_{sh} [ms^{-1}]	n	α	K_{sv} [ms^{-1}]
1	1.5	0.4032	0.0505	5.18E-06	1.4673	14.37	5.18E-09
2	0.8	0.4314	0.0654	5.60E-06	1.5934	16.64	5.60E-09
3	0.8	0.4179	0.0594	3.58E-06	1.5516	16.17	3.58E-09
4	1.5	0.4283	0.0762	9.10E-07	1.4146	18.37	9.11E-10
5	1.0	0.3885	0.0413	4.00E-06	1.4139	12.80	4.00E-09
6	0.8	0.3885	0.0413	4.00E-06	1.4139	12.80	4.00E-09
7	0.8	0.4195	0.0706	1.01E-06	1.4376	18.25	1.01E-09
8	1.5	0.4326	0.0688	7.54E-06	1.5741	17.52	7.54E-09
9	0.8	0.3995	0.0482	4.88E-06	1.4540	13.98	4.88E-09
10	0.6	0.4347	0.0644	5.09E-06	1.6172	16.00	5.09E-09
11	0.8	0.4222	0.0707	1.12E-06	1.4506	17.99	1.12E-09

Table 7 – Calibrated soil parameters value, Carson River

Class	Depth [m]	ϑ_s	ϑ_r	K_{sh} [ms^{-1}]	n	α	K_{sv} [ms^{-1}]
1	0.80	0.4576	0.0839	6.42E-05	2.5000	22.39	2.53E-07
2	1.10	0.4490	0.0779	1.50E-04	2.5000	20.87	2.63E-06
3	1.75	0.3883	0.0414	7.27E-05	2.5000	12.77	2.86E-07
4	1.15	0.2331	0.0413	1.35E-04	2.5000	12.80	5.99E-07
5	0.85	0.4058	0.0592	5.22E-04	2.5000	14.31	1.37E-06
6	1.15	0.4045	0.0572	3.44E-05	2.5000	16.86	4.64E-07
7	1.25	0.4326	0.0688	1.27E-04	2.5000	17.52	5.02E-07
8	1.70	0.4032	0.0505	8.75E-05	2.5000	14.37	3.45E-07
9	1.00	0.3885	0.0413	6.76E-05	2.5000	12.80	1.78E-07

Table 8 – Calibrated soil parameters value, American River

Class	Depth [m]	ϑ_s	ϑ_r	K_{sh} [ms^{-1}]	n	α	K_{sv} [ms^{-1}]
1	0.93	0.4032	0.0505	3.35E-05	2.5000	14.37	4.23E-08
2	1.00	0.4314	0.0654	5.47E-04	2.5000	16.64	3.25E-07
3	0.79	0.4179	0.0594	7.67E-05	2.5000	16.17	1.51E-07
4	0.88	0.4283	0.0762	1.82E-04	2.5000	18.37	2.73E-07
5	0.75	0.3885	0.0413	2.50E-05	2.5000	12.80	3.49E-08
6	0.65	0.3885	0.0413	2.50E-05	2.5000	12.80	3.49E-08
7	0.78	0.4195	0.0706	7.63E-05	2.5000	18.25	9.26E-07
8	1.15	0.4326	0.0688	1.05E-04	2.5000	17.52	2.25E-06
9	1.10	0.3995	0.0482	9.71E-05	2.5000	13.98	1.22E-07
10	0.70	0.4347	0.0644	1.02E-04	2.5000	16.00	7.65E-07
11	0.90	0.4222	0.0707	2.24E-05	2.5000	17.99	1.68E-07

Tables 9,10 – Channel (left) and Evapo-transpiration and Snowmelt (right) parameters value, Carson River and American River

Carson River and American River							
Strahler Order	1	2	3	4	5	6	7
Manning Coefficient	0.075	0.065	0.055	0.050	0.045	0.040	0.035
River Bed Angle	1.5	2.2	2.7	3.2	3.7	4.5	6

	Carson River	American River
β_1	0.30	0.30
β_2	0.90	0.85
T_s [°C]	1.5	1.8

The availability of the Snow Water Equivalent (SWE) measurement allows to evaluate the model capability to reproduce the snow accumulation and melting process. For the Carson River this component is critical, because the mean elevation is greater than 2000 m and the hydrological process is driven mainly by the snow accumulation and melting process. The following evaluation indexes for the SWE comparison are computed: Bias, Root Mean Square Error (*RMSE*), Correlation Coefficient (*r*) and Modified Correlation Coefficient (r_{mod}).

3.3.1 American River

American River at North Fork Dam is rich of events during the calibration period; its hydrological regime is various and it includes many rain and mixed rain and snow events. The events reported in Table 10 are shown in the Figures 10-19 and along with their evaluation indexes are shown. The comparison between the calibrated and uncalibrated series and the respective indexes reveals that the uncalibrated model overestimates the flood events; the calibrated model evaluation indexes, instead, are good both in individual flood events and in long-term periods. The calibration of the model allows to well reproduce the flood and the low water events. In Figures 11 and 15, the snow melting process is visible and the modeled behavior is very similar to the observed one.

Table 10 – American River: events and corresponding figures

Start Time	End Time	Peak [m^{3}s^{-1}]	Figure
07/03/1989 00:00	15/03/1989 00:00	334	**10**
01/03/1989 00:00	13/05/1989 00:00	334	**11**
01/03/1991 00:00	08/03/1991 00:00	507	**12**
07/01/1995 00:00	19/01/1995 00:00	751	**13**
09/03/1995 00:00	13/03/1995 00:00	631	**14**
06/04/1995 00:00	19/06/1995 00:00	463	**15**
04/02/1996 00:00	09/02/1996 00:00	550	**16**
16/01/1996 00:00	26/05/1996 00:00	550	**17**
26/12/1996 00:00	05/01/1997 00:00	1818	**18**
04/12/1996 00:00	12/02/1997 00:00	1818	**19**

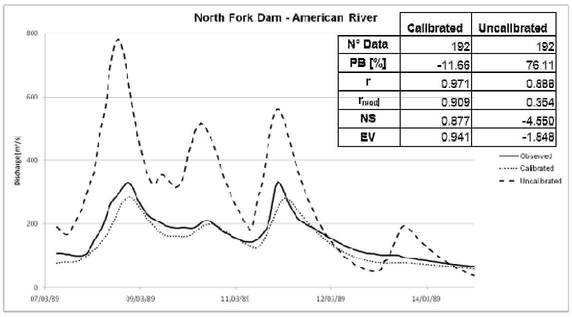

Figure 10

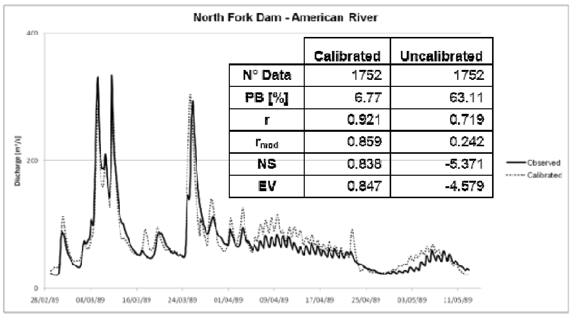

Figure 11

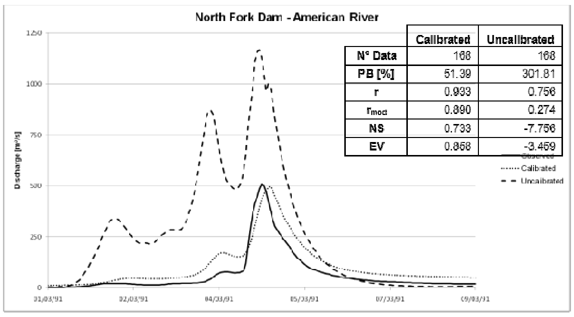

Figure 12

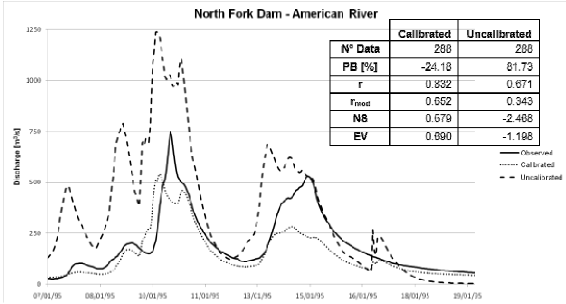

Figure 13

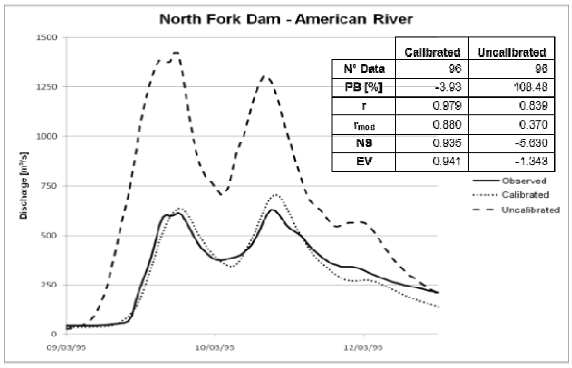

Figure 14

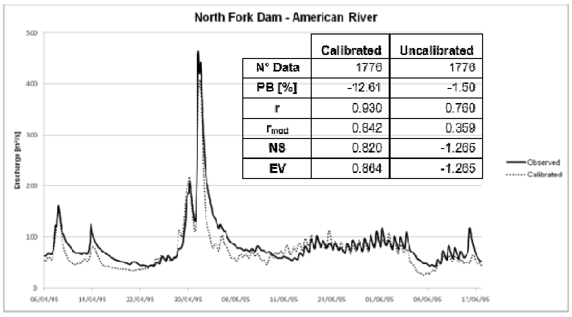

Figure 15

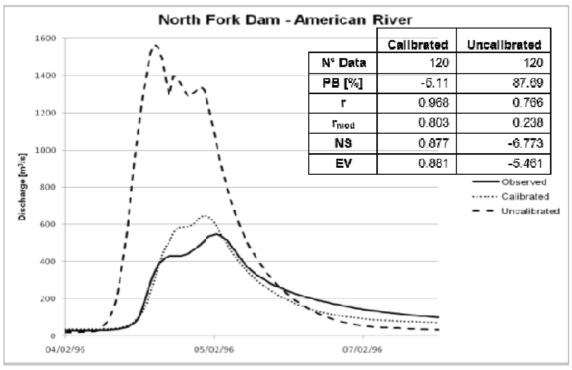

Figure 16

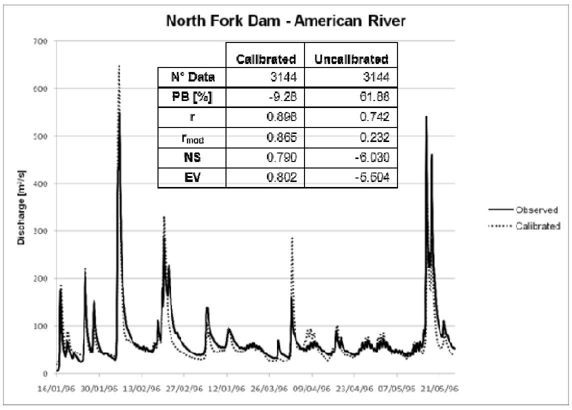

Figure 17

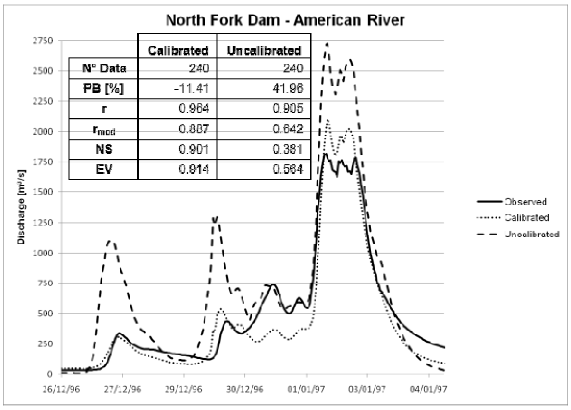

Figure 18

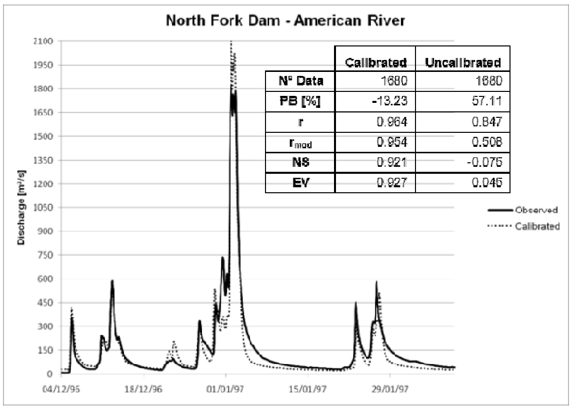

Figure 19

Table 11 – American River: yearly and overall statistics for North Fork Dam measurement station

YEAR	N° Data	Peak [m^3s^{-1}]	PB [%]	r	r_{mod}	NS	EV
1989	8308	334	27.0	0.95	0.92	0.87	0.90
1990	8759	89	55.0	0.90	0.71	0.47	0.69
1991	7052	507	61.0	0.93	0.78	0.68	0.79
1992	8783	164	93.8	0.86	0.62	0.11	0.47
1993	8711	487	9.4	0.92	0.88	0.84	0.84
1994	8759	129	106.3	0.82	0.47	-0.90	-0.15
1995	8759	751	-16.6	0.92	0.80	0.83	0.85
1996	8783	738	0.4	0.91	0.83	0.83	0.83
1997	6527	1818	-9.3	0.98	0.97	0.95	0.95
ALL	75936	1818	12.9	0.94	0.89	0.88	0.89

The yearly and overall indexes (Table 11) show that the flood events are well reproduced on the whole calibration period and they are worst in years without significant flood events and better when the yearly peak is large.
The event statistic indexes (Table 13) confirm the good behavior of the model on the flood events, showing a great improvement after the model calibration.

Table 12 – American River: selected events for event statistics

Event	Start Time	End Time	Peak [m^3s^{-1}]
1	08/03/1989 00:00	10/03/1989 00:00	331
2	11/03/1989 08:00	13/03/1989 00:00	334
3	24/03/1989 00:00	28/03/1989 00:00	294
4	01/03/1991 00:00	08/03/1991 00:00	507
5	20/01/1993 00:00	22/01/1993 00:00	374
6	22/01/1993 00:00	24/01/1993 00:00	484
7	07/01/1995 00:00	13/01/1995 00:00	751
8	13/01/1995 00:00	17/01/1995 00:00	532
9	09/03/1995 00:00	10/03/1995 19:00	615
10	10/03/1995 19:00	13/03/1995 14:00	632
11	01/05/1995 03:00	04/05/1995 00:00	463
12	04/02/1996 00:00	09/02/1996 00:00	550
13	01/01/1997 00:00	05/01/1997 00:00	1818

Table 13 – American River: event statistics for North Fork Dam measurement station

North Fork Dam - American River		
	Calibrated	Uncalibrated
N° Events	13	13
ER [%]	13.43	78.77
EP [%]	17.18	101.45
ET [h]	4.00	7.31

Table 14 – American River: Snow Water Equivalent statistics for Blue Canyon measurement station

Blue Canyon - American River - 1610 m					
	N°Data	BIAS [mm]	RMSE [mm]	r	r_{MOD}
1988	105	-23.6	38.6	0.922	0.789
1989	163	-35.4	48.4	0.987	0.742
1990	131	-32.4	51.1	0.913	0.664
1991	243	-3.9	15.4	0.978	0.807
1992	112	-4.7	46.9	0.59	0.39
1993	325	-23.6	52.9	0.988	0.772
1994	318	-29.6	57.8	0.885	0.291
1995	337	-57.2	128.7	0.224	0.054
1996	362	-9.3	29.2	0.889	0.518
ALL	2419	-24	62.9	0.848	0.589

Table 15 – American River: Snow Water Equivalent statistics for Huysink measurement station

Huysink - American River - 2012 m					
	N°Data	BIAS [mm]	RMSE [mm]	r	r_{MOD}
1988	137	-287	316	0.542	0.268
1989	202	-153	229.8	0.766	0.753
1990	208	-116	177.4	0.69	0.33
1991	313	-92.6	157.5	0.708	0.324
1992	225	-145	221.7	0.339	0.187
1993	276	-34.3	205.5	0.909	0.858
1994	300	-134	222.3	0.663	0.208
1995	230	-174	347.9	0.875	0.422
1996	365	-122	246	0.791	0.462
ALL	2576	-115	224.6	0.81	0.697

The snow accumulation and melting module of the TOPKAPI model is simple and it requires only one parameter: the snow formation temperature threshold. The American River basin mean elevation is low and in winter the temperature is often close to 0° C, so the uncertainty about the real status of the precipitation is high and some rain events are mistaken for snow events and vice versa; this behavior is clearly visible in Figure 13. The SWE statics evaluation indexes (Tables 14 and 15) are not so good, especially for the lower measurement station, Blue Canyon. Nevertheless, due to the low elevation of the basin, the snow accumulation and melting component is not very significant, hence the TOPKAPI model well reproduces the flood events for the most part of the period of simulation.

3.3.2 Carson River

The Carson River hydrological regime is mainly determined by the snow accumulation and melting process; on the whole calibration period there are few great floods events and the snow melting during the spring and summer seasons is the main event in many years. In this basin, the making process of the flood events is influenced mainly by the quantity of snow that melts and infiltrates in the soil. This quantity is significant for the determination of the soil saturation state: if it is underestimated and a significant rain event occurs, the consequent flood event will be underestimated and the opposite happens when the soil saturation is overestimated.

On this river the model behavior is variable: in some years the snow melting occurs late (Figures 20 and 25), in other years it is on time (Figures 24 and 30) or in advance (Figure 22 and 27). Nevertheless, the individual event evaluation indexes are quite good and similar are the events statistics (Tables 19 and 21) and the yearly and overall statistics indexes (Table 17 and 20); also on this basin the years with the main floods events have better results.

Where the elevation is high, the temperature is often lower than 0° C, and the precipitation is often snow; this is the reason of the good SWE indexes (Tables 22-25), especially on the higher measurement stations.

Table 16 – Carson River: events and corresponding figures for both the calibration stations, respectively Gardnerville and Markleevilee

Start Time	End Time	Peak [m^3s^{-1}]	Figure
05/01/1993 00:00	26/07/1993 00:00	74 - 84	**20, 25**
09/03/1995 00:00	13/03/1995 00:00	168 - 167	**21, 26**
24/04/1995 00:00	24/07/1995 00:00	113 - 145	**22, 27**
22/04/1996 00:00	18/06/1996 00:00	200 - 221	**23, 28**
25/12/1996 00:00	12/01/1997 00:00	527	**29**
16/03/1997 00:00	26/06/1997 00:00	61 - 63	**24,30**

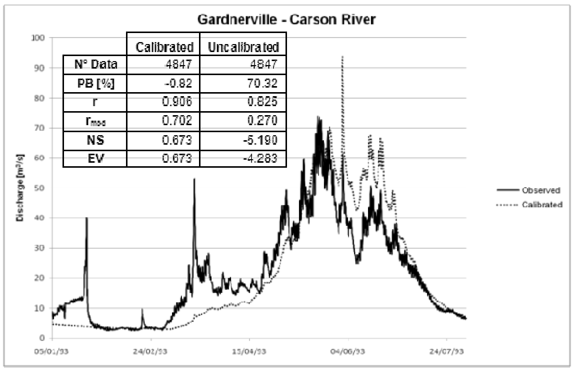

Figure 20

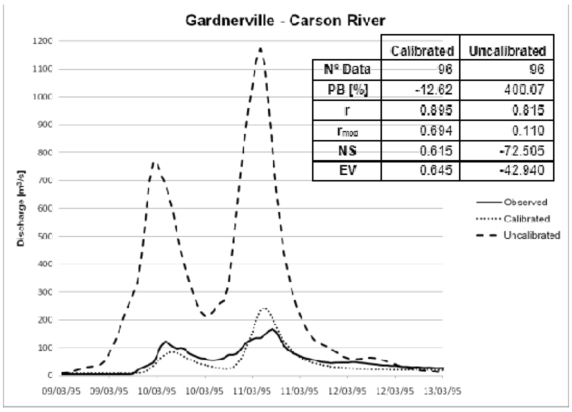

Figure 21

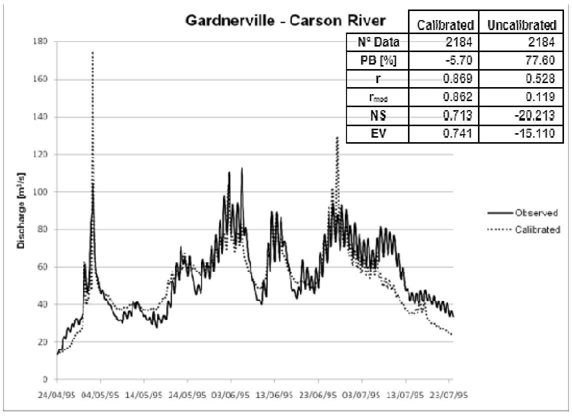

Figure 22

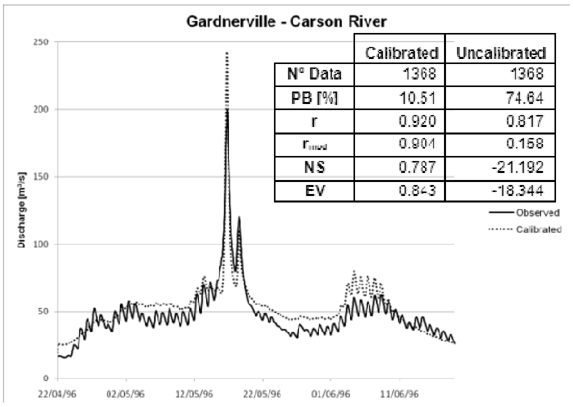

Figure 23

Table 17 – Carson River at Gardnerville: yearly and overall statistics

YEAR	N° Data	Peak [m^{3}s^{-1}]	PB [%]	r	r_{mod}	NS	EV
1991	8755	38	88.2	0.85	0.47	-0.72	-0.23
1992	8776	27	137.8	0.94	0.44	-2.12	-0.55
1993	8756	84	-1.7	0.92	0.83	0.81	0.81
1994	8758	31	79.3	0.92	0.50	-0.46	0.02
1995	8520	167	-19.2	0.95	0.81	0.86	0.89
1996	8685	221	3.5	0.93	0.86	0.86	0.86
1997	6415	527	0.8	0.90	0.72	0.80	0.80
ALL	60869	527	13.9	0.89	0.81	0.79	0.80

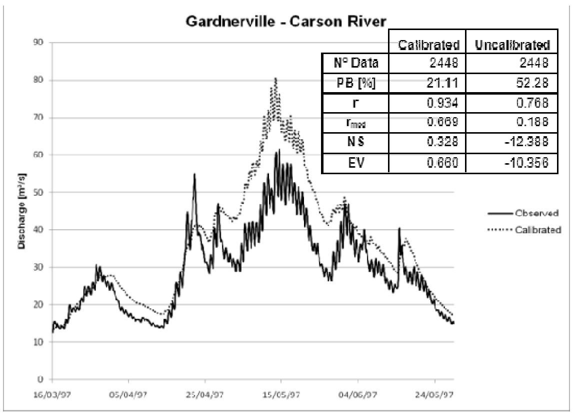

Figure 24

The model behavior on both the measurement stations is similar. The Markleeville station is upstream with respect to the Gardnerville station and it includes the main event registered on the whole calibration period (Figure 29), missed by the Gardnerville station. This event is underestimated by the model and it has a different shape, probably due to the presence of the snow.
It has to be noticed that the calibration at Gardnerville is the best one as well for Markleeville. This means that the TOPKAPI model is able to well reproduce the behavior of the river also in points different from the calibration one. This is a great feature of the TOPKAPI model and it highlights the physical bases of the model and the respect of the physical meaning of the parameters.

Table 18 – Carson River: selected events for event statistics, for both the calibration stations, respectively Gardnerville and Markleeville

Event	Start Time	End Time	Peak [m^{3}s^{-1}]
1	09/03/1995 00:00	10/03/1995 14:00	124 – 153
2	10/03/1995 14:00	12/03/1995 00:00	168 – 167
3	01/05/1995 00:00	04/05/1995 00:00	105 – 134
4	15/05/1996 15:00	18/05/1996 00:00	200 – 221
5	26/12/1996 00:00	06/01/1997 00:00	NA - 527

Table 19 – Carson River: event statistics for Gardnerville measurement station

Gardnerville - Carson River		
	Calibrated	**Uncalibrated**
N° Events	4	4
ER [%]	6.26	329.48
EP [%]	38.34	699.20
ET [h]	1.50	2.75

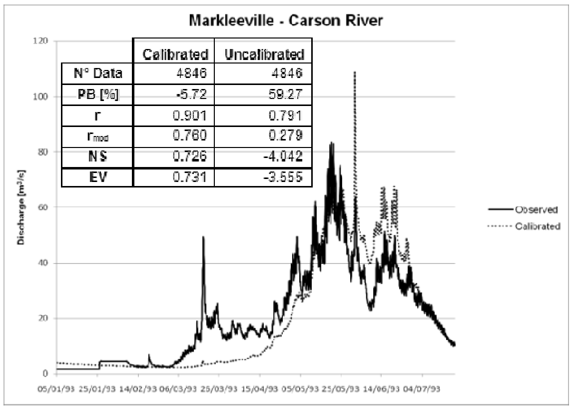

Figure 25

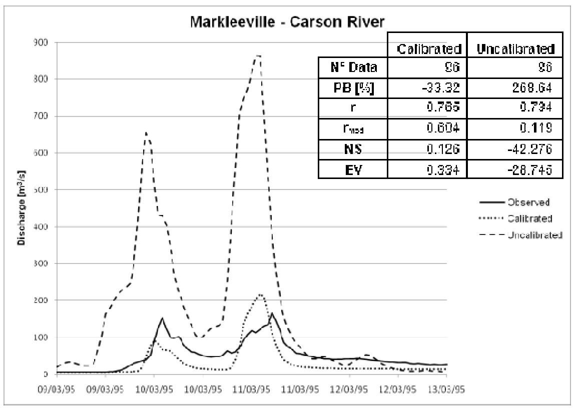

Figure 26

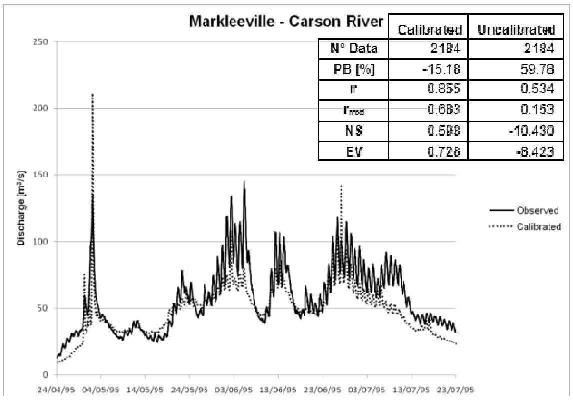

Figure 27

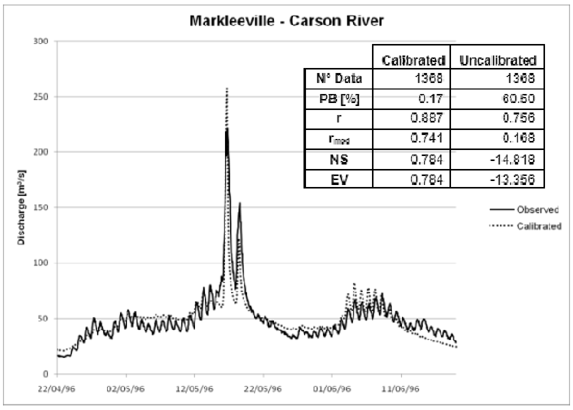

Figure 28

Table 20 – Carson River at Markleerville: yearly and overall statistics

YEAR	N° Data	Peak [m^{3}s^{-1}]	PB [%]	r	r_{mod}	NS	EV
1991	8743	39	102.3	0.84	0.44	-1.28	-0.46
1992	8782	27	160.5	0.93	0.40	-3.51	-1.02
1993	8757	74	3.5	0.92	0.79	0.79	0.79
1994	8733	32	110.0	0.94	0.47	-1.20	-0.23
1995	8253	168	-7.7	0.96	0.92	0.91	0.92
1996	8669	200	19.2	0.93	0.91	0.84	0.86
1997	4997	385	13.5	0.94	0.83	0.88	0.88
ALL	59125	385	28.0	0.91	0.91	0.79	0.82

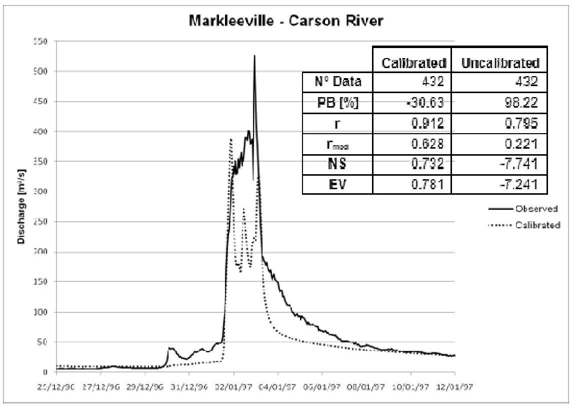

Figure 29

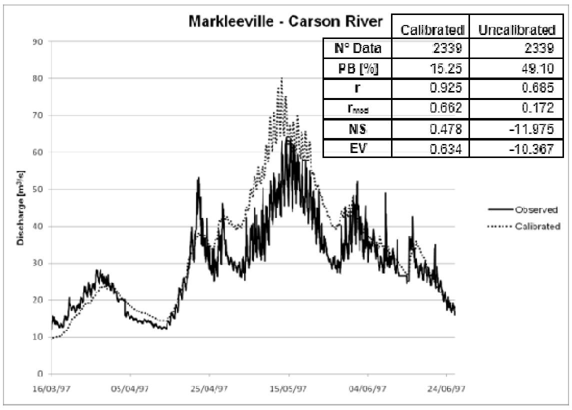

Figure 30

Table 21 – Carson River: event statistics for Markleeville measurement station

Markleeville - Carson River		
	Calibrated	**Uncalibrated**
N° Events	5	5
ER [%]	24.75	211.43
EP [%]	30.28	382.71
ET [h]	7.20	7.80

Table 22 – Carson River: Snow Water Equivalent statistics for Spratt Creek measurement station

Spratt Creek - Carson River - 1864 m					
	N°Data	**BIAS [mm]**	**RMSE [mm]**	**r**	**r_{MOD}**
1990	364	17.2	38	0.893	0.468
1991	364	37.4	64.7	0.739	0.26
1992	365	10.4	27.2	0.964	0.558
1993	364	110.4	198.5	0.863	0.424
1994	364	15.4	33.4	0.94	0.559
1995	364	95	160.9	0.762	0.242
1996	365	47.2	84.5	0.76	0.283
ALL	2915	49.7	108.7	0.832	0.354

Table 23 – Carson River: Snow Water Equivalent statistics for Poison Flats measurement station

Poison Flats - Carson River - 2358 m					
	N°Data	**BIAS [mm]**	**RMSE [mm]**	**r**	**r_{MOD}**
1990	364	-0.9	6.9	0.998	0.988
1991	364	24.1	46.7	0.963	0.793
1992	365	14.5	27.7	0.994	0.769
1993	364	3.2	41.1	0.989	0.983
1994	363	-1.1	23.4	0.978	0.941
1995	364	-20.1	69.4	0.973	0.868
1996	365	12.6	40.7	0.974	0.934
ALL	2914	12.2	56.9	0.957	0.916

Table 24 – Carson River: Snow Water Equivalent statistics for Ebbets Pass measurement station

Ebbets Pass - Carson River - 2672 m					
	N°Data	BIAS [mm]	RMSE [mm]	r	r_{MOD}
1990	364	-11.7	26.3	0.988	0.974
1991	364	45.2	99.1	0.955	0.717
1992	365	11.3	21.9	0.997	0.946
1993	364	70.9	112.6	0.989	0.901
1994	364	37.1	51.6	0.996	0.843
1995	364	-6.7	37.9	0.999	0.97
1996	365	6.1	36.3	0.996	0.993
ALL	2915	22.4	65.8	0.991	0.964

Table 25 – Carson River: Snow Water Equivalent statistics for Blue Lakes measurement station

Blue Lakes - Carson River - 2456 m					
	N°Data	BIAS [mm]	RMSE [mm]	r	r_{MOD}
1990	364	-52.2	105.9	0.822	0.665
1991	364	-2.7	52.2	0.969	0.893
1992	365	-17.2	69.7	0.933	0.918
1993	364	-38.7	160.3	0.941	0.929
1994	364	2.3	79.7	0.907	0.794
1995	364	-58.6	203	0.949	0.921
1996	365	-16.6	116.2	0.938	0.937
ALL	2915	-19	118.7	0.953	0.943

4 CONCLUSION

The hydrological physically based and fully distributed TOPKAPI model has been applied to the Sierra Nevada basins within the DMIP 2 Project. The two used basins are quite different: Carson River basin has an high mean elevation and its hydrological regime is mainly influenced by the snow melting process; American River basin is lower and it has a more complex hydrological regime with many flood events during the year and the snow melting process is less significant.

On the American River the streamflow series is well reproduced, even if, due to the winter temperature, often close to 0° C, some rain events are mistaken for snow events and vice versa. Nevertheless, both the overall and the event evaluation indexes are optimal.

Carson River basin's mean elevation is high and the snow melting process is the main component of its hydrological regime; the accuracy of the model snow melting module is a critical factor to obtain good model performance. One of the tests requested in the DMIP 2 modeling instruction was to calibrate the model at the downstream section, Gardnerville, without using the observed streamflow data at the upstream section, Markleeville, and afterwards it was requested to calibrate the model at Markleeville. The model has been calibrated at Gardnerville and the simulation at Markleeville was produced. This simulation well reproduces the river behavior and calibrating at Markleeville best results are not obtained. The possibility to have simulations also in ungauged interior points of the basin is one of the distributed model benefits with respect to a non distributed model. The obtained results demonstrate that the TOPKAPI model is capable to reproduce these simulations with good performance.

Another benefit of the distributed models is the ability to reproduce streamflow also in entirely ungauged basins, using the parameters value available in literature. In this application, the comparison between the calibrated and uncalibrated simulations shows that using literature parameters value gives poor performance and that flood events are always overestimated; this is mainly due to the low values of the horizontal and vertical conductivities. The sub-surface flow occurs in the superficial soil layer, not composed by compact terrain, as the literature parameters value referred to. Hence, it is reasonable to use, as uncalibrated parameters, values of horizontal and vertical conductivities greater than the literature ones. Good knowledge and experience on calibrating the model allows to obtain good performance also in ungauged basins. The comparison between calibrated and uncalibrated soil parameters (Tables 5 and 7 for Carson River and Tables 6 and 8 for American River) shows that the calibration concerned mainly the soil thickness and conductivities, The latters are about 1 or 2 orders of magnitude greater than the uncalibrated values and this is a common behavior encountered in most of the model applications. Thus, often is sufficient to increase these values without calibrating the model to obtain reasonable performances.

REFERENCES

Abbott, M. et al., 1986a. An introduction to the European Hydrological System – Système Hydrologique Européen, SHE; 1. History and philosophy of a physically based distributed modeling system, Journal of Hydrology, Vol. 87, 45-59. 2. Structure of a physically based, distributed modeling.

Abbott, M. et al., 1986b. Physically-based distributed modelling of an upland catchment using the Système Hydrologique Européen . Journal of Hydrology, Vol. 87: 79-102.

Anderson, E. A., 1968, "Development and Testing of Snow Pack Energy balance equations," Water Resources Research, 4(1): 19-37.

Anderson, E. A., 1976, "A Point Energy and Mass Balance Model of a Snow Cover," NOAA Technical report NWS 19, U.S. Department of Commerce.

Band, L.E.. 1986. Topographic partition of watersheds with digital elevation models. Water Resour. Res., 22(1): 15-24.

Benning R.G., 1994. Towards a new lumped parameterization at catchment scale. Doctoral thesis.

Beven K.J., Germann P.. 1982. Macropores and water flow in soils. Water Resour. Res., 18(5): 1311-1325.

Beven K.J., 1981. Kinematic subsurface stormflow. Water Resour. Res., 17(5): 1419-1424.

Beven K.J.. 1982. On subsurface stormflow: prediction with simple kinematic theory for saturated and

unsaturated flows. Water Resour. Res., 18(6): 1627-1633.
Blöschl G., Sivapalan M., 1995. Scale issues in hydrological modelling: a review. Hydrol. Proc., 9: 251-290.
Borah, D. K., Prasad, S. N., Alonso, C. V., 1980. Kinematic wave routing incorporating shock fitting. Water Resources Research, 16(3), pp. 529-541.
Bras, R. L., 1990. Hydrology, An introduction to hydrologic science, Addison-Wesley, Reading, MA, 643 p.
Cash, J.R., and Karp, A. H., 1990. A variable order Runge-Kutta method for initial value problems with rapidly varying right hand sides. ACM Transactions on Mathematical Software, 16(3):201-222.
Charbonneau, R., J. P. Lardeau and O. C, 1981. Problems of modelling a high mountainous drainage basin with predominant snow yields, Hydrological Sciences Bulletin, 26(4): 345-361.
Chow, V. T., Maidment, D. R., and Mays, L. W., 1988. Applied Hydrology, McGraw-Hill, NY, New York.
Chow, V. T., 1964. Handbook of Applied Hydrology, McGraw-Hill, NY, New York.
Clapp, R.B., Hornberger, G.M., 1978. Empirical equations for some soil properties. Water Res. Res., 14, 601-604.
Colbeck, S. C., 1978. The physical aspects of water flow through snow, Advances in Hydroscience, 11.34
Colbeck, S. C., 1991. The layered character of snow covers, Reviews of Geophysics, 29(1): 81-96.
Cunge J.A., 1969. On the subject of flood propagation method (Muskingum method). Jour. Hydraulic Research, ASCE, 7(2):205-230.
de Marsily, Ghislain, 1986. Quantitative hydrology: Groundwater Hydrology for Engineers. Chapter 11 - Geostatistic and stochastic approach in hydrogeology. Academic Press, Inc., California, p286-329
Dingman, S. L., 1994. Physical Hydrology, Macmillan, 575 p.
Doorembos J., Pruitt W.O., Aboukhaled A., Damagnez J., Dastane N.G., van den Berg C., Rijtema P.E., Ashford O.M., Frere M., 1984. Guidelines for predicting crop water requirements. FAO Irrig. Drainage Pap., 24.
Dozier, J., 1979. A Solar Radiation Model for a Snow Surface in Mountainous Terrain, in Proceedings Modeling Snow Cover Runoff, ed. S. C. Colbeck and M. Ray, U.S. Army Cold Reg. Res. Eng. Lab., Hanover, NH, p.144-153.
Dozier, J., 1987. Recent research in Snow Hydrology, Reviews of Geophysics, 25(2): 153- 161.
Henderson F.M., Wooding R.A.. 1964. Overland flow and groundwater flow from a steady rainfall of finite duration. J. Geophys. Res., 69(6): 1531-1540.
Hurley D.G., Pantelis G.. 1985. Unsaturated and saturated flow through a thin porous layer on a hillslopes. Water Resour. Res., 21(6): 821-824.
Jeton, A.E., Dettinger, M.D., and Smith, J.L., 1996. Potential effects of climate change on streamflow, Eastern and Western slopes of the Sierra Nevada, California and Nevada. U.S. Geological Survey Water Resources Investigations Report 95-4260, 44 pp.
Koussis A.D., 1980. Comparison of Muskingum method difference schemes. Jour. Hydraulics Division, ASCE, 106(5):925-929.
Koussis A.D., 1983. Accuracy criteria in diffusion routing: a discussion. Jour. Hydraulic Engineering, ASCE, 109(5):803-806.
Leavesley, G. H., A. M. Lumb and L. G. Saindon, 1987. A microcomputer-based watershedmodeling and data-management system," in 55th Annual meeting, Western Snow Conference, April 14-17, p.108-117.
Leu, C. H., 1988. Evaluation of Spatially-Distributed snowpack estimation using pattern recognition, PhD Thesis, Civil and environmental engineering, Utah State University.
Linsley, R. K., M. A. Kohler and J. L. H. Paulhus, 1975. Hydrology for Engineers, 2nd Edition, McGraw-Hill, Kogakusha, Ltd, 482 p.
Liu Z., 2002. Toward a comprehensive distributed/lumped rainfall-runoff model: Analysis of available physically-based models and proposal of a new TOPKAPI model. PhD Dissertation. University of Bologna.
Liu Z., Martina M. L. V., Todini E., 2005. Flood forecasting using a fully distributed model: application of the TOPKAPI model to the Upper Xixian Catchment. Hydrology and Earth System Sciences, 9, 347-364
Liu, Z., Todini, E., 2001. Towards a comprehensive physically-based rainfall-runoff model, Hydrology and Earth System Sciences, 6, 859-881.
Maidment, D.R., 1993. Handbook of Hydrology, McGraw-Hill, New York.
Male, D. H. and D. M. Gray, 1981. Snowcover Ablation and Runoff, Chapter 9 in Handbook of Snow, Principles, Processes, Management and Use, Edited by D. M. Gray and D. H. Male, Pergammon Press, p.360-436.
Marshall, S. E. and S. G. Warren, 1987, Parameterization of snow albedo for climate models, in Large Scale Effects of Seasonal Snowcover, Proceedings of the Vancouver Symposium, IAHS Publ. no. 166.
Matheron, G., 1970. La théorie des variables regionaliséés et ses applications, Cah. Cent. Morphol. Math., 5.
McCarthy, G. T., 1940. Flood Routing, Chap. V of “Flood Control”, The Engineer School, Fort Belvoir, Virginia, pp. 127–177.
McCarthy, G. T., 1938. The Unit Hydrograph and Flood Routing. Unpublished manuscript presented at a conference of the North Atlantic Division, U.S. Army, Corps of Engineers.
Miller, W.A., Cunge, JA, 1975. Simplified equations of unsteady flow. Unsteady flow in open channels, by K. Mahamood and V. Yevjevixh, Water Resource Publication, Ft. Collins, Colo.

Morris, E. M., 1982. Sensitivity of the European Hydrological System snow models," in Hydrological Aspects of Alpine and High Mountain Areas, Proceedings of the Exeter Symposium, IAHS Publ no 138, p.221-231.

Nash, J.E., and J.V. Sutcliffe, 1970. River flow forecasting through conceptual models: Part I - A discussion of principles. J. Hydrol., 10, 282-290.

Perumal, M., O'Connell, P. E., and Ranga Raju, K. G., 2001. Field Applications of a Variable Parameter Muskingum Method, J. Hydrol. Eng.-ASCE, 6(3), 196–207.

Ponce V.M., Yevjevich V., 1978. Muskingum-Cunge methods with variables parameters. Jour. Hydraulics Division, ASCE, 104(HY12):1663-1667.

Prince RK, 1995. Flood routing. In Development in Hydraulics Engineering, 3, [Ed. P. Novak], Elsevier,129-173.

Reed, S., Koren V., Smith M., Zhang Z., Moreda F., Seo D. J., 2004. Overall distributed model intercomparison project results. Jour. Hydrol., 298:27-60.

Sloan, P.G., Moore I.D.. 1984. Modeling subsurface stormflow on steeply sloping forested watersheds. Water Resour. Res., 20(12): 1815-1822.

Smith, AA, 1980. Generalized approach to kinematic flood routing. Jour. Hydrol., 45(1-2):71-89.

Smith, M. B., Seo, D. J., Koren, V., Reed, S., Zhang, Z., Duan, Q., Moreda, F., Cong, S.. 2004, The distributed model intercomparison project (DMIP): motivation and experiment design. Jour. Hydrol. 298:4-26.

Smith, M., Koren, V., Reed, S., Zhang, Z., Seo, D.J., Moreda, F., Cui, Z., 2006. The Distributed Model Intercomparison Project: Phase 2, Science Plan, www.weather.gov/oh/hrl/dmip/2/science_plan.html.

Stagnitti F., Parlange M.B., Steenhuis T.S., Parlange J.Y., 1986. Drainage from a uniform soil layer on a hillslope. Water Resour. Res., 22(5): 631-634.

Steenhuis T.S., Parlange J.Y., Parlange M.B., Stagnitti F., 1988. A simple model for flow on hillslopes. Agric. Water Manage., 14(5): 153-168.

Tang X, Samuels PG, 1999. Variable parameter Muskingum-Cunge method for flood routing in a compound channel. Jour. Hydraulic Research, 37:591-614.

Thornthwaite, C.W. and Mather, J.R., 1955. The water balance. Publ. in Climatology, 8(1) Lab. of Climatology, Centerton, N.J.

Todini E., 1995. New trends in modeling soil processes from hill-slope to GCMS Scales - The role of water and the hydrological cycle in global change, edited by H. R. Oliver, S. A. Oliver, NATO ASI Series I: Global Environmental Change, 31: 317-347.

Todini E., 2007. A mass conservative and water storage consistent variable parameter Muskingum-Cunge approach. Hydrol. Earth Syst. Sci., 11:1645–1659.

Todini, E., Ciarapica L., 2001. The TOPKAPI model. Mathematical Models of Large Watershed Hydrology, Chapter 12, edited by Singh. V.P. et al., Water Resources Publications, Littleton, Colorado.

Todini. E., 1996. The ARNO rainfall-runoff model. J. Hydrology ,175, p339-382.Wood, E. F.,

U.S. Army Corps of Engineers, 1956. Snow Hydrology, Summary report of the Snow Investigations, U.S. Army Corps of Engineers, North Pacific Division, Portland, Oregon.

Van Genuchten, M.Th.. 1980. A closed form for predicting the Hydraulic conductivity of unsaturated soils, Soil Sci. Soc. Am. J. 44:892-898

Viessman, W., G. L. Lewis and J. W. Knapp, 1989. Introduction to Hydrology, 3rd Edition, Harper & Row.

Wienmann PE, Laurenson EM, 1979. Approximate flood routing methods: a review. Jour. Hydraulics Division, ASCE, 105(12):1521-1536.

Wigmosta M.S., Vail, L.W. and Lettenmier, D.P., 1994. A distributed hydrology-vegetation model for complex terrain. Water Resources Research, Vol. 30, No. 6: 1165-1679.

Wiscombe, W. J. and S. G. Warren, 1981. A Model of the Spectral Albedo of Snow. I: Pure Snow, Journal of the Atmospheric Sciences, 37: 2712-2733.

Wooding, R.A., 1965. A hydraulic modeling of the catchment-stream problem. 1. Kinematic wave theory. Journal of Hydrology, 3:254-267.